Eur. Phys. J. D **20**, 469–480 (2002)
DOI: 10.1140/epjd/e2002-00147-6

THE EUROPEAN PHYSICAL JOURNAL D

Interaction between aromatic amine cations and nonpolar solvents: Infrared spectra of isomeric aniline$^+$–Ar$_n$ (n = 1, 2) complexes

N. Solcà and O. Dopfer[a]

Institut für Physikalische Chemie, Universität Basel, Klingelbergstrasse 80, 4056 Basel, Switzerland

Received 4 February 2002
Published online 13 September 2002 –

Abstract. Infrared (IR) photodissociation spectra of the aniline$^+$–Ar$_n$ cations, An$^+$–Ar$_n$ ($n = 1, 2$), are analyzed in the vicinity of the N–H stretch fundamentals. The complexes are produced in an electron impact (EI) ion source which produces predominantly the most stable cluster isomers. Two isomers of An$^+$–Ar are identified by their characteristic N–H stretch frequencies: the planar proton-bound global minimum, in which the Ar ligand forms a nearly linear H-bond to the amino group, and the less stable π-bound local minimum, in which the Ar atom is attached to the π-electron system of the aromatic ring. This result is the first unambiguous detection of the most stable H-bound An$^+$–Ar dimer. All previous spectroscopic studies of An$^+$–Ar employed resonance enhanced multiphoton ionization (REMPI) of neutral An–Ar and identified only the less stable π-bound cation due to restrictions arising from the Franck-Condon principle. The EI-IR spectrum of An$^+$–Ar$_2$ shows that the most stable structure of this trimer features two equivalent H-bonds (C_{2v} symmetry). The interpretation of the experimental data is supported by quantum chemical calculations. The *ab initio* potential of An$^+$–Ar calculated at the UMP2/6-311G(2df, 2pd) level features H-bound global minima ($D_e = 513$ cm^{-1}) and π-bound local minima ($D_e = 454$ cm^{-1}), with a barrier of $V_b \approx 140$ cm^{-1} for isomerization from the π-bound toward the H-bound minimum.

PACS. 36.40.Mr Spectroscopy and geometrical structures of clusters – 36.40.Wa Charged clusters – 34.20.Gj Intermolecular and atom-molecule potentials and forces

1 Introduction

Intermolecular forces are of fundamental importance for many biophysical phenomena, such as protein folding and molecular recognition [1–4]. Ion–ligand interactions play often a dominant role for these phenomena because they are significantly stronger and of longer range than the corresponding interactions between neutral species [5–10]. For example, large biomolecular units are often (multiply) charged due to (de-)protonation or charge separation processes, or they possess metal ion centers solvated by biomolecular ligands (*e.g.*, hemoglobin) [4]. In particular, the additional electrostatic, induction, and charge transfer interactions caused by the excess charge lead to large solvation energies of an ion surrounded by solvent molecules [5–10].

In the past, ionic complexes isolated in the gas phase have extensively been used to investigate the properties of ion–ligand interaction potentials by mass spectrometric and spectroscopic methods [7–11]. In the present work, the interaction of the aniline cation (An$^+$) in its ground electronic state with surrounding Ar ligands is characterized by infrared (IR) spectroscopy and quantum chemical calculations of An$^+$–Ar$_n$ complexes. Aniline is the simplest aromatic amine and offers several competing binding sites. For example, ligands can bind to the π-electron system of the aromatic ring (π-bond), the H atoms of the amino group (H-bond), the N atom of the amino group (N-bond), or the H atoms of the aromatic ring (H^C-bond). The preferred binding site depends strongly on the type of ligand (polar or nonpolar) and the degree of electronic excitation and charge state of An [12–15]. Hence, the An$^+$–Ar$_n$ complexes are suitable model systems to characterize the intermolecular interaction between an aromatic amine cation with a nonpolar solvent. Such interactions are relevant for biophysical processes where charged amines interact with a hydrophobic environment [4].

Spectroscopic and theoretical studies show that the neutral An monomer is pyramidal in its ground electronic state (S_0) with an inversion barrier of 450–560 cm^{-1} [16–22], whereas the first excited singlet state (S_1) [20–24] as well as the cation ground state (D_0) [25–32] have (quasi-)planar equilibrium structures. Neutral An–Ar$_n$ complexes (n = 1–11) have been studied in the S_0 and S_1 states by various spectroscopic techniques. The results relevant for the present work can

[a] e-mail: otto.dopfer@unibas.ch

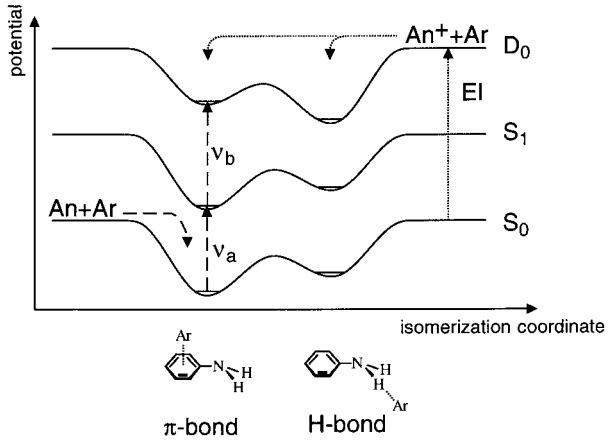

Fig. 1. Sketch of potential energy curves of An–Ar in various electronic states (S_0, S_1, D_0). The dashed arrows indicate the preparation of An^+–Ar cations in the D_0 state by resonance enhanced multiphoton ionization (REMPI). The neutral precursor is formed in a supersonic expansion in the neutral ground state (S_0) and ionized by resonant two-photon one-color ($\nu_a = \nu_b$) or two-color ($\nu_a \neq \nu_b$) ionization *via* the intermediate S_1 state. The dotted arrows indicate the generation of An^+–Ar by electron impact (EI) ionization of bare An and subsequent dimerization in the expansion.

be summarized as follows. Spectra at the level of rotational resolution reveal that the An–Ar dimer ($n = 1$) has a π-bound equilibrium structure in both the S_0 and S_1 states (Fig. 1) [21,33–36], in agreement with theoretical potentials [37–42] and low-resolution electronic spectra [38,43–48]. In the S_0 state, the Ar ligand is located ≈3.5 Å above the aromatic plane of pyramidal An (*anti* conformer) and slightly displaced from the center of the ring toward the N atom [21,33,35,36]. High level *ab initio* calculations at the MP2 level yield a well depth of $D_e \approx 400$ cm^{-1} [41], compatible with the most recent experimental dissociation energy of $D_0 = 301 \pm 28$ cm^{-1} [31]. The energy difference between the lower lying *anti* and higher lying *syn* conformers is predicted to be small (<20 cm^{-1} [41]). The intermolecular interaction in the S_1 state increases by 53 cm^{-1}, leading to a somewhat shorter intermolecular bond ($\Delta R \approx -0.1$ Å [21,33]). No spectroscopic and theoretical evidence for a less stable H-bound An–Ar isomer in the S_0 and S_1 states has been reported so far. However, similar to the isoelectronic Ph–Ar dimer [49], H-bound An–Ar may be a shallow local minimum on the intermolecular potential energy surface (PES) of the S_0 state, and *ab initio* calculations discussed in Section 3 confirm this anticipation. The vibronic analysis of low-resolution $S_1 \leftarrow S_0$ excitation spectra of An–Ar_2 [38,43,47,50,51], including band shifts of the electronic origin as well as the intermolecular vibrational structure confirms the existence of two isomers: the (1|1) isomer has two equivalent π-bound Ar ligands attached on opposite sides of the aromatic ring (with little interaction between the two Ar ligands), whereas they are on the same side in the less stable (2|0) isomer. This interpretation is supported by semiempirical potential calculations [37,38,52]. The electronic $S_1 \leftarrow S_0$ spectra of larger An–Ar_n clusters ($n = 3$–6 [37,38,47]) reveal the coexistence of several ($k|m$) isomers (with $k+m = n$), having k Ar atoms on one side of the aromatic plane and m Ar atoms on the other side. Again, the identification of isomers is based on the analysis of S_1 band shifts and intermolecular vibrational structure as well as potential calculations. Interestingly, all Ar ligands in An–Ar_n (up to $n = 6$) are located in roughly planar Ar solvation layers above and below the aromatic ring and there is no evidence for any H-bound Ar ligand. According to the observed and calculated incremental S_1 band shifts, the Ar ligands can be classified according to binding to the π-electron system, above the amino group and above peripherical C–H bonds [38,47,48]. IR spectra of An–Ar and the (1|1) isomer of An–Ar_2 [31,53] are consistent with π-bound dimer and (1|1) trimer structures in both the S_0 and S_1 states. Moreover, the IR spectrum of An in a cryogenic Ar matrix between 500 and 4 000 cm^{-1} is similar to the gas-phase spectrum of bare An [54].

The intermolecular interaction in the D_0 ground electronic state of An^+–Ar_n complexes ($n = 1$–5) has been investigated by photoionization efficiency (PIE) measurements [55–57], zero kinetic energy photoelectron (ZEKE) spectroscopy [27–29], and resonance enhanced multiphoton ionization coupled with IR spectroscopy (REMPI-IR) [31,53]. The complexation-induced shifts in the ionization potentials (IPs) are characteristic for different structural isomers and Ar ligand binding sites. Again, the Ar ligands have been classified according to binding to the π-electron system, above the amino group and above peripherical ring hydrogens [56,57]. For example, the π-bound dimer features a red shift of ΔIP ≈ −110 cm^{-1} [27,28,57] and the corresponding shift for the (1|1) trimer is approximately twice that of the dimer (ΔIP ≈ −220 cm^{-1}), consistent with two equivalent π-bound Ar ligands attached to opposite sides of the aromatic ring [27,28]. The REMPI-IR spectrum of π-bound An^+–Ar allowed the binding energy of the π-bond in the cation ground state to be determined as 414±28 cm^{-1} [31]. Although the dissociation energy of this isomer increases upon ionization (by *ca.* 110 cm^{-1}), the intermolecular potential along the b_x coordinate becomes flatter leading to a smaller frequency for the symmetric bending mode, ν_{bx} (ν_{bx} is the intermolecular bending vibration along the axis of the amino group): $\nu_{bx} = 22$ and 16 cm^{-1} in the S_1 and D_0 states, respectively [27–29,38,44,48]. Moreover, extended progressions in the ν_{bx} mode dominate the ZEKE spectra of π-bound An^+–Ar in the intermolecular frequency range, indicating a substantial shift of the Ar ligand toward the amino group upon ionization [27,28]. In addition to the IP shifts, the analysis of both the inter- and intramolecular vibrational frequencies of the π-bound An^+–Ar dimer and (1|1) An^+–Ar_2 trimer observed in the ZEKE [27–29] and REMPI-IR [31,53] spectra are compatible with equivalent intermolecular π-bonds.

Prior to the present work, all spectroscopic studies of the An^+–Ar_n cation clusters in the D_0 state are based on resonant photoionization of the corresponding neutral

precursors [27–29,31,53,55–57]. In the case of isoelectronic phenol$^+$–Ar$_n$ (Ph$^+$–Ar$_n$) clusters, it was recently demonstrated that REMPI techniques for the generation of the most stable cluster ions suffer from the severe restrictions imposed by the Franck-Condon (FC) principle [58–60]. Similar limitations apply to the An$^+$–Ar$_n$ clusters produced in a REMPI ion source, as shall briefly be discussed by considering the potential diagrams of the An–Ar dimer shown in Figure 1. According to the *ab initio* calculations described in Section 3, An–Ar has a π-bound global minimum (in agreement with all experimental data), whereas the H-bound structure is a less stable isomer (which so far has escaped experimental identification). Consequently, An–Ar dimers formed in a cold supersonic jet have predominantly a π-bound structure and subsequent resonant two-photon one-color ($\nu_a = \nu_b$) or two-color ($\nu_a \neq \nu_b$) ionization *via* the S_1 state leads (almost) exclusively to the formation of π-bound An$^+$–Ar dimers because the FC principle implies vertical transitions (dashed arrows in Fig. 1). Thus, all spectroscopic studies of An$^+$–Ar based on REMPI techniques have observed only the π-bound isomer and no signature of the H-bound cation has been identified. However, the quantum chemical calculations presented in Section 3 clearly show that the π-bound An$^+$–Ar cation is only a local minimum on the intermolecular PES, whereas the H-bound structure is in fact the global minimum. As both minima are well separated by a significant potential barrier, the FC factors for populating the H-bound global minimum *via* REMPI of the neutral π-bound global minimum nearly vanish.

To overcome the restrictions of the REMPI cluster ion source, the present work employs for the first time electron impact ionization (EI) in a supersonic expansion for the production of An$^+$–Ar$_n$ clusters. In the EI cluster ion source, An molecules are first ionized by electron impact and cold An$^+$–Ar$_n$ clusters are formed by subsequent three-body association reactions in the collision region of the expansion (dotted arrows in Fig. 1 for $n = 1$). Hence, in contrast to the REMPI source, the EI source is not limited by the FC principle and generates predominantly the most stable An$^+$–Ar$_n$ clusters (*e.g.*, the H-bound isomer for $n = 1$) and in smaller concentrations less stable isomers (*e.g.*, the π-bound dimer). IR spectra of the Ph$^+$–Ar cation demonstrated the principle differences of both cluster ion sources for the spectroscopic characterization of ionic complexes. The REMPI-IR spectrum of Ph$^+$–Ar reveals only absorptions of the less stable π-bound isomer and no signature of the global H-bound minimum is observed [61,62]. In contrast, the EI-IR spectrum is dominated by absorptions of the global H-bound minimum and under warm conditions also transitions of the less stable π-bound dimer are detected [58–60]. Thus, the major goal of the present work is the characterization of the intermolecular interaction of An$^+$–Ar$_n$ ($n = 1,\ 2$) clusters in the cation ground state by EI-IR spectroscopy in the vicinity of the N–H stretch vibrations. Of particular interest is the competition between H-bonding and π-bonding and the comparison with the corresponding REMPI-IR spectra reported in reference [53]. Moreover, the intermolecular PES of An$^+$–Ar is investigated in some detail by *ab initio* and density functional calculations, as no previous theoretical studies of the cation PES are available in the literature.

2 Experimental

IR photodissociation spectra of mass-selected An$^+$–Ar$_n$ complexes ($n = 1, 2$) are recorded in a tandem mass spectrometer described elsewhere [63]. Briefly, An$^+$–Ar$_n$ complexes are produced in a pulsed supersonic expansion of a heated An sample ($T \approx 60°$) seeded in Ar at a backing pressure of 6–8 bar. Electron impact ionization of the An/Ar gas mixture close to the nozzle orifice is followed by ion-molecule and clustering reactions to form ionic complexes. The central part of the plasma is extracted through a skimmer into a quadrupole mass spectrometer, which is tuned to the mass of An$^+$–Ar$_n$. Subsequently, the mass selected parent beam is injected into an octopole ion guide, where it is overlapped with a tunable IR laser pulse. Resonant excitation into vibrational levels above the dissociation threshold leads to fragmentation of An$^+$–Ar$_n$ according to the following photodissociation process:

$$\mathrm{Ar^+{-}Ar}_n + h\nu_{\mathrm{IR}} \rightarrow (\mathrm{An^+{-}Ar}_n)^* \rightarrow \mathrm{An^+} + n\mathrm{Ar}. \quad (1)$$

No other fragment channel upon resonant excitation in the 3 μm range is observed for $n = 1$ and $n = 2$. The An$^+$ fragment ions produced are selected by a second quadrupole mass spectrometer and detected as a function of the laser frequency to obtain the photodissociation spectrum of An$^+$–Ar$_n$. Tunable IR radiation is created by a pulsed optical parametric oscillator laser system with a bandwidth of 0.02 cm^{-1}. Frequency calibration accurate to better than 0.2 cm^{-1} is accomplished by recording optoacoustic spectra of ammonia [64] simultaneously with the IR action spectra. All photodissociation spectra are normalized for laser intensity variations measured with an InSb detector.

Similar to the related Ph$^+$–Ar$_n$ clusters [58–60], the main production pathway of the An$^+$–Ar$_n$ cation complexes in the EI ion source is thought to begin with electron impact (or Penning) ionization of An followed by three-body association reactions (dotted path in Fig. 1). Thus, this ion source produces predominantly the most stable isomer of a given cluster size (global minimum on the PES) and to a smaller extent less stable isomers (local minima on the PES).

3 Quantum chemical calculations

Quantum chemical *ab initio* and density functional calculations [65] are carried out for An$^+$–Ar$_n$ ($n = 0$–2) at the UMP2(fc)/6-311G(2df, 2pd) and B3LYP/6-31G* levels of theory to investigate the intermolecular interaction between An$^+$ and Ar as well as the effects of Ar complexation on the properties of An$^+$. Of particular interest are the characterization of global and local minima (structure, binding energy, vibrational frequencies and

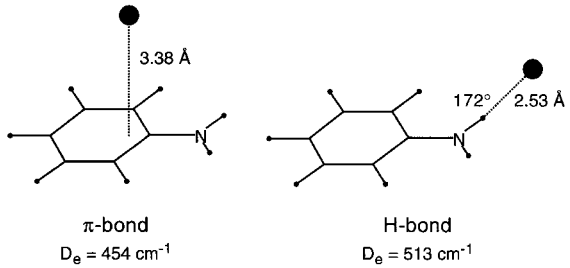

Fig. 2. Equilibrium structures of the planar H-bound global minimum and the π-bound local minimum of An^+–Ar calculated at the UMP2/6-311G(2df, 2pd) level. Both geometries have C_s symmetry. Dissociation energies (D_e), intermolecular separations (R_e), and intermolecular bond angles (φ_e) are indicated.

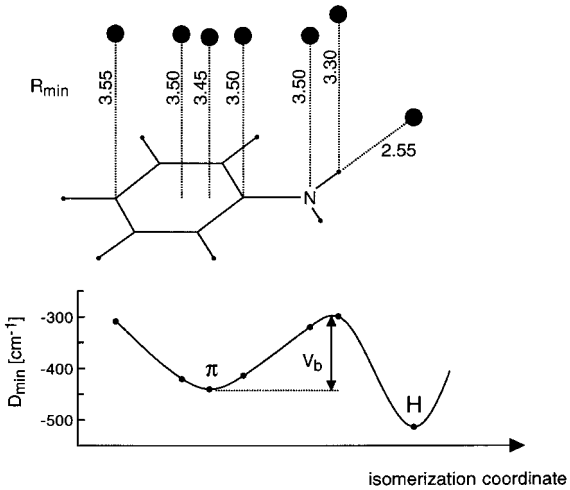

Fig. 3. Minimum energies (D_{min}) and intermolecular separations (R_{min}, in Å) of 1D radial cuts through the 3D intermolecular potential energy surface of An^+–Ar calculated at the UMP2/6-311G(2df, 2pd) level (rigid monomer approximation). The calculated data points are interpolated by a polynomial fit to estimate the potential barrier, V_b, along the isomerization coordinate.

IR intensities) as well as isomerization barriers between these minima. Previous UMP2 calculations for the isoelectronic Ph^+–Ar dimer show that the 6-311G(2df, 2pd) basis set systematically underestimates the intermolecular interaction strength but correctly reproduces the shape of the potential and the relative stability of structural isomers [58,59]. Consequently, this level is chosen for evaluating the interaction energies of the An^+–Ar dimer. In general, all coordinates are relaxed during the search for stationary points and all interaction and dissociation energies are counter-poise corrected for basis set superposition error [66].

In agreement with previous experimental and theoretical studies, An^+ is found to have a planar structure with C_{2v} symmetry in its $^2B_1$ (D_0) ground electronic state [25–28,30–32]. Similar to Ph^+–Ar [58–60], the planar H-bound An^+–Ar dimer corresponds to the global minimum of the potential (D_e = 513 cm^{-1}), whereas the π-bound isomer is a less stable local minimum (D_e = 454 cm^{-1}). Both equilibrium structures have C_s symmetry and the relevant structural parameters and dissociation energies of the intermolecular bonds in the two minima obtained with gradient optimization are listed in Figure 2. The planar H-bound dimer has a slightly *cis*-linear hydrogen bond ($\varphi_e = 172°$) and an intermolecular H–Ar separation of R_e = 2.53 Å. In the π-bound local minimum the Ar ligand is separated by 3.38 Å from the aromatic plane and significantly shifted from the ring center toward the N atom. In the cation D_0 state the Ar atom is closer to the amino group compared to neutral An–Ar (in both the S_0 and S_1 states). This result agrees with the long progressions of the intermolecular bending vibration along the axis of the NH_2 group (ν_{bx}) observed in the ZEKE spectra of π-bound An^+–Ar [27–29]. The calculated well depth of π-bound An^+–Ar, D_e = 454 cm^{-1}, is compatible with the experimental dissociation energy, $D_0 = 414 \pm 28$ cm^{-1} [31].

In order to estimate the lowest-energy isomerization path and corresponding barrier height between the π-bound and H-bound An^+–Ar minima, several one-dimensional (1D) radial cuts through the 3D intermolecular potential are calculated at the UMP2/6-311G(2df, 2pd) level (Fig. 3). In these calculations the An^+ geometry is kept frozen at the optimal monomer structure (rigid monomer approximation). Interaction energies are calculated in steps of 0.05 Å along various radial paths either perpendicular to or in the An^+ plane. The minimum energies (D_{min}) and corresponding intermolecular distances (R_{min}) of the considered 1D cuts are summarized in Figure 3. As expected, only little differences are observed between D_{min} (rigid monomer, Fig. 3) and D_e (relaxed monomer, Fig. 2) for the two minima because the weak intermolecular bonds cause only small structural relaxation of the intramolecular An^+ coordinates upon Ar complexation. The lowest-energy isomerization path from the π-bound toward the H-bound minima can be summarized as follows: starting from the π-bound local minimum ($D_{min} \approx 440$ cm^{-1}, $R_{min} \approx 3.45$ Å), the Ar atom moves more or less parallel to the aromatic plane *via* the *ipso* C atom ($D_{min} \approx 410$ cm^{-1}, $R_{min} \approx 3.50$ Å) and the N atom ($D_{min} \approx 320$ cm^{-1}, $R_{min} \approx 3.50$ Å) toward one H atom of the amino group ($D_{min} \approx 300$ cm^{-1}, $R_{min} \approx 3.30$ Å) before it reaches the global minimum in the molecular plane at the H-bound structure ($D_{min} \approx 510$ cm^{-1}, $R_{min} \approx 2.55$ Å). Other isomerization paths considered (not included in Fig. 3) appear to have higher barriers. For example, $D_{min} \approx 340$ and ≈ 290 cm^{-1} for the Ar atom located above the C atom in *ortho* position and the corresponding H atom, respectively. Thus, the lowest isomerization barrier is estimated to be of the order of $V_b \approx 140$ cm^{-1} and occurs above the N–H bond. A barrier of $V_b > 100$ cm^{-1} is consistent with the ZEKE spectra of π-bound An^+–Ar [27–29] which show quite regular and harmonic progressions in the intermolecular bending vibration along the isomerization path ($n\nu_{bx}$ = 16, 32, 47, and 65 cm^{-1} for n = 1–4, respectively).

Table 1. Properties of An$^+$–Ar$_n$ ($n = 0$–2) calculated at the B3LYP/6-31G* level: frequencies (scaling factor 0.95663) and IR intensities (km/mol, in parentheses) of ν_s and ν_a, frequency shifts with respect to bare An$^+$ ($\Delta\nu_{s,a}$), and complexation-induced changes in the N–H bond length ($\Delta r_{\mathrm{N-H}}$).

An$^+$–Ar$_n$	$\Delta r_{\mathrm{N-H}}$[a] [Å]	ν_s [cm^{-1}]	$\Delta\nu_s$ [cm^{-1}]	ν_a [cm^{-1}]	$\Delta\nu_a$ [cm^{-1}]
$n = 0$		3 388.1 (253)		3 490.7 (89)	
$n = 1$ (H-bound)	0.0016	3 374.0 (359)	−14.1	3 479.3 (134)	−11.4
	0.0001				
$n = 1$ (π-bound)	0.0001	3 386.8 (251)	−1.3	3 489.3 (88)	−1.4
$n = 2$ (HH)	0.0015	3 366.8 (443)	−21.3	3 468.5 (219)	−22.2

[a] $r_{\mathrm{N-H}} = 1.0156$ Å for bare An$^+$.

In order to estimate the complexation-induced vibrational frequency shifts for An$^+$–Ar$_n$ ($n = 1,\ 2$), calculations are carried out at the B3LYP/6-31G* level. Previous studies for Ph$^+$–Ar [58] demonstrated that this theoretical level qualitatively reproduces inter- and intramolecular bond properties of the H-bound complex, such as bond lengths and vibrational frequencies, although the dissociation energies are somewhat underestimated compared to the UMP2 level. The results relevant for the present work are collected in Table 1 and further details are available upon request. The harmonic frequencies are scaled by a factor 0.95663 to optimize the agreement between the experimental [67] and calculated N–H stretch fundamentals of bare An$^+$. Both N–H stretch local modes are equivalent in the An$^+$ monomer and the resonant interaction gives rise to symmetric and antisymmetric N–H stretch normal modes, ν_s and ν_a, respectively. The coupling is relatively strong and produces a splitting of 103 cm^{-1} between ν_a and ν_s. In H-bound An$^+$–Ar, complexation significantly weakens the N–H bond adjacent to the intermolecular bond and the bound N–H bond length increases substantially ($\Delta r_1 = 0.0016$ Å), whereas the free N–H bond is almost unchanged ($\Delta r_2 = 0.0001$ Å). The weak intermolecular bond reduces somewhat the coupling between the two local N–H oscillators but the decoupling is far from being complete due to the small intermolecular perturbation. Thus, the frequencies of both the ν_s and ν_a modes in H-bound An$^+$–Ar are reduced upon complexation, $\Delta\nu_s = -14$ cm^{-1} and $\Delta\nu_a = -11$ cm^{-1}. As expected, the shift of ν_s is slightly larger than for ν_a, as the corresponding normal mode features a larger contribution of the bound N–H stretch (*ca.* 60 *vs.* 40%). The enhancement in the IR intensity upon H-bonding is similar for both modes (42 *vs.* 51%). Both N–H stretch oscillators are again equivalent in the planar An$^+$–Ar$_2$ trimer featuring two intermolecular proton bonds (HH isomer, C_{2v} symmetry). However, the N–H bonds in An$^+$–Ar$_2$ are longer ($\Delta r = 0.0015$ Å) than in bare An$^+$. Accordingly, both ν_s and ν_a display similar total red shifts with respect to bare An$^+$ ($\Delta\nu_s = -21$ cm^{-1}, $\Delta\nu_a = -22$ cm^{-1}). The decrease in the average frequency of the N–H stretch modes upon sequential Ar complexation is nearly additive (−13 and −22 cm^{-1}) implying that three-body forces are small and noncooperative. The IR intensity of both N–H stretch fundamentals in An$^+$–Ar$_2$ are roughly by a factor 2 larger than in An$^+$. In contrast to H-bonding, π-bound Ar ligands have almost no effect on the properties of the N–H bonds. Consequently, the calculated N–H stretch fundamentals of the π-bound An$^+$–Ar isomer have essentially the same frequencies and IR intensities as in An$^+$. Although the B3LYP/6-31G* level severely underestimates the interaction for π-bonding, the properties of the amino group are not expected to change significantly upon complexation at this binding site [13,31,53,58–60]. Indeed, the experimental N–H stretch frequencies of An$^+$ [67] and π-bound An$^+$–Ar [53] agree to within 2 cm^{-1} (Tab. 2).

In order to elucidate the origin of the interaction in the An$^+$–Ar dimer, the charge distribution of An$^+$ is analyzed using the atoms-in-molecules (AIM) population analysis [65]. The AIM atomic charges at the UMP2 and B3LYP levels are $+0.12e$ for ring H atoms, $+0.6e$ for the *ipso* C atom, ≈0 for other C atoms, $-1.2e$ for N, and $+0.5e$ for the amino H atoms. Thus, the attraction at the H-bound global minimum is dominated by the charge-induced dipole interaction, mainly caused by the high positive partial charge on the amino proton engaged in the intermolecular N–H···Ar bond. In contrast, the main attraction in the π-bound geometry is coming from dispersion interaction between the π-electron system of the aromatic ring and the electrons of Ar. A significantly smaller contribution comes from induction, mainly induced by the positive partial charge on the *ipso* C atom. This contribution causes the Ar atom to shift away from the center of the aromatic ring toward the NH_2 substituent. The fact that the dissociation energy of the π-bound structure increases only moderately upon ionization (≈40% [31]) confirms that dispersion forces provide the major contribution to the attraction in the π-bound cation.

Despite the numerous experimental and theoretical studies on neutral An–Ar$_n$ complexes [21,31,33–48,50–53,55–57], the possibility of H-bonding of Ar to the amino group has never been explored. Calculations of the isoelectronic Ph–Ar dimer show that the H-bound dimer is a local minimum in the S_0 state [49]. Thus, calculations at the MP2(fc)/6-311G(2df, 2pd) level have been performed for An–Ar to test the relative stability of the H-bound and π-bound dimers in the S_0 state. Harmonic frequency analysis confirms that both isomers are indeed minima on the neutral PES, with the π-bond being substantially more stable than the nearly linear H-bond ($\varphi_e \approx 177°$): $D_e = 365$ *vs.* 94 cm^{-1}, $R_e = 3.35$ *vs.* 2.70 Å. Thus, the qualitative potential diagrams in Figure 1 for the S_0 and D_0 state are confirmed by *ab initio* calculations. However, it is unclear which structure is more stable in the S_1 state.

Table 2. Band maxima, widths (fwhm), complexation shifts (all in cm^{-1}) and suggested assignments of the vibrational transitions observed in the EI-IR photodissociation spectra of An^+–Ar_n. In addition, corresponding data obtained from REMPI-IR spectra are listed for comparison.

n	EI-IR	shift[a]	assignments	REMPI-IR[b]	shift[a]
1	3 270 (6)		$2\nu_b(NH_2)$		
	3 381 (6)	−12	ν_s of H-bound An^+–Ar		
	3 389 (6)		$\nu_s + \nu_i \leftarrow \nu_i$ of H-bound An^+–Ar[c]		
	3 395 (6)	2	ν_s of π-bound An^+–Ar	3 394.5 (3)	1.5
	3 477 (6)	−9	ν_a of H-bound An^+–Ar		
	3 483 (4)		$\nu_a + \nu_i \leftarrow \nu_i$ of H-bound An^+–Ar[c]		
	3 489(4)	3	ν_a of π-bound An^+–Ar	3 488 (3)	2
2	3 373 (9)	−20	ν_s of HH An^+–Ar_2		
	3 462 (6)	−24	ν_a of HH An^+–Ar_2		
			ν_s of $\pi\pi$ An^+–Ar_2	3 395.0 (<4.5)	2
			ν_a of $\pi\pi$ An^+–Ar_2	3 489.8 (<4.5)	3.8

[a] Frequency shifts are calculated with respect to the transitions of bare An^+ at $\nu_s = 3\,393\ cm^{-1}$ and $\nu_a = 3\,486\ cm^{-1}$ (Ref. [67]). [b] References [13,53]. [c] Tentative assignments.

According to the calculations, ionization has a rather different effect on the interaction energy of both isomers: the binding energy increases by a factor of 1.2 and 5.4 for π-bound and H-bound An–Ar, respectively.

In summary, the calculations suggest that the H-bound dimer corresponds to the global minimum of the An^+–Ar PES, whereas the π-bound isomer represents a local minimum. As both isomers are separated by a substantial isomerization barrier, they may be produced with detectable abundance in the EI cluster ion source because of their similar dissociation energies. Moreover, both An^+–Ar isomers can readily be distinguished by their characteristic N–H stretch frequencies although the predicted complexation shifts are small.

4 Experimental results and discussion

4.1 An^+–Ar dimer

Figure 4 compares the IR spectra of An^+–Ar produced in the present EI source (a, b) and by one-color two-photon (1+1) REMPI (c and d [53]). Table 2 collects the band maxima, widths, and suggested assignments of the transitions observed in the EI-IR spectrum of An^+–Ar between 3 130 and 3 600 cm^{-1} (Fig. 4a). An expanded view of the EI-IR spectrum in the range of the N–H stretch vibrations is shown in Figure 4b. The most intense transitions at 3 381 and 3 477 cm^{-1} in the EI-IR spectrum are unambiguously assigned to the ν_s and ν_a fundamentals of H-bound An^+–Ar, because they are significantly shifted to lower frequency compared to the corresponding vibrations of bare An^+ (indicated by arrows in Fig. 4, $\nu_s = 3\,393\ cm^{-1}$, $\nu_a = 3\,486\ cm^{-1}$ [67]). The H-bound dimer corresponds to the global minimum on the calculated An^+–Ar PES and is expected to be the most abundant isomer in the expansion. The observed complexation shifts of H-bound

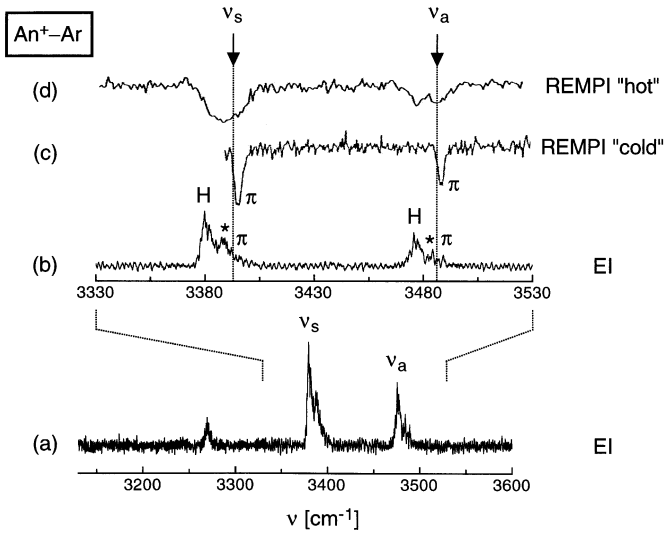

Fig. 4. IR photodissociation spectra of An^+–Ar. (a) Overview of the EI-IR spectrum between 3 130 and 3 600 cm^{-1}. (b) Expanded view of the EI-IR spectrum in the range of the N–H stretch vibrations, ν_s and ν_a. (c) REMPI-IR spectrum of "cold" An^+–Ar generated by 1+1 REMPI of neutral An–Ar (reproduced from Ref. [53]). (d) REMPI-IR spectrum of "hot" An^+–Ar generated by 1+1 REMPI of neutral An–Ar_2 and subsequent fragmentation (reproduced from Ref. [53]). The arrows indicate the positions of the ν_s and ν_a fundamentals of bare An^+ (3 393 and 3 486 cm^{-1} [67]). The bands marked by asterisks are attributed to sequence transitions. The assignments of all transitions are listed in Table 2.

An^+–Ar, $\Delta\nu_s = -12\ cm^{-1}$ and $\Delta\nu_a = -9\ cm^{-1}$, are similar to the calculated values of −14 and −11 cm^{-1}, respectively. Moreover, the experimental ratio of the intensities of ν_s and ν_a (≈2) is in qualitative agreement with the calculated one (≈2.7). The red shifts $\Delta\nu_{s/a}$ correspond

to the increase in the intermolecular binding energy upon vibrational excitation. Assuming a dissociation energy of the order of ≈500 cm^{-1} for H-bound An$^+$–Ar (Fig. 2), the increase is ≈2–3% for the $\nu_{s/a}$ vibrational states. The change in binding energy is similar for both vibrations because the weak intermolecular interaction does not significantly reduce the coupling between the two local N–H stretch modes. The assignments to the H-bound isomer are confirmed by the analysis of the rotational band profiles. Excitation of a proton donor stretch gives rise to a shorter and stronger intermolecular bond. The bond contraction causes the rotational constants in the excited state to be larger than in the ground state, leading to the appearance of a blue shaded band contour with a sharp head in the P branch [10,58,68,69]. Such a contour is clearly observed for ν_s and to a smaller degree also for ν_a of H-bound An$^+$–Ar, because both modes contain significant bound N–H stretch character.

The EI-IR spectrum of An$^+$–Ar in Figure 4b is qualitatively different from the corresponding REMPI-IR spectrum in Figure 4c. The latter spectrum was obtained by generating An$^+$–Ar *via* 1+1 REMPI of neutral An–Ar [53] and this process produces mainly the less stable π-bound An$^+$–Ar dimer (Fig. 1). Consequently, the corresponding IR spectrum reveals only the absorptions of this isomer and the transitions of the most stable H-bound isomer are completely absent. Because 1+1 REMPI excitation *via* the S_1 origin of π-bound An–Ar generates rotationally and vibrationally "cold" π-bound An$^+$–Ar cations [27,28], the IR transitions are relatively narrow [53]. The ν_s and ν_a frequencies of π-bound An$^+$–Ar are reported as 3 394.5 and 3 488 cm^{-1} [53] and display only small blue shifts of 1–2 cm^{-1} compared to the transitions of bare An$^+$ [67] (Tab. 2). Such small blue shifts are expected for π-bonding because Ar complexation at the aromatic ring has little influence on the properties of the N–H bonds (Tab. 1). For comparison, the corresponding blue shifts for ν_1 (O–H stretch) of π-bound Ph$^+$–Ar and Ph$^+$–Kr are also of the order of 1–2 cm^{-1} [58–62]. In the EI-IR spectrum of Ph$^+$–Ar, both the π-bound local minimum (D_e = 396 cm^{-1}) and the H-bound global minimum (D_e = 656 cm^{-1}) are observed under the present experimental conditions [58–60]. The difference in the calculated binding energies of both An$^+$–Ar isomers (ΔD_e = 59 cm^{-1}) is much smaller than for the corresponding Ph$^+$–Ar isomers (ΔD_e = 260 cm^{-1} [58]) at the UMP2/6-311G(2df, 2pd) level. Hence, as the calculated barriers to isomerization in An$^+$–Ar and Ph$^+$–Ar are comparable (V_b ≈ 140–150 cm^{-1}), it is probable that the π-bound An$^+$–Ar isomer is also produced with significant abundance in the present EI ion source. Closer inspection of the EI-IR spectrum in Figure 4b reveals indeed very weak absorptions in the region of the $\nu_{s/a}$ fundamentals of the π-bound local minimum (Tab. 2).

In addition to the ν_s and ν_a fundamentals of the H-bound and π-bound isomers, the EI-IR spectrum of An$^+$–Ar reveals "satellite" bands at 3 388 and 3 483 cm^{-1}, occurring in the blue wings of both N–H stretch fundamentals of H-bound An$^+$–Ar (indicated by asterisks in Fig. 4b). They may either be attributed to sequence transitions of H-bound An$^+$–Ar involving $\nu_{s/a}$ or to the $\nu_{s/a}$ fundamentals of less stable isomers. Sequence transitions of the type $\nu_{s/a} + \nu_i \leftarrow \nu_i$, where ν_i are intermolecular modes, are typical for excitation of proton donor stretch vibrations [58,68,69]. These sequence transitions occur as satellite transitions with higher frequency than the $\nu_{s/a}$ fundamentals, because the stronger intermolecular interaction in the vibrationally excited states leads to higher intermolecular frequencies. The frequencies of the intermolecular stretching and the two bending modes of H-bound An$^+$–Ar are calculated as 57, 31, and 15 cm^{-1}, respectively. Consequently, the 8 and 6 cm^{-1} spacings between the $\nu_{s/a}$ fundamentals and $\nu_{s/a}+\nu_i \leftarrow \nu_i$ transitions (Tab. 2) would imply that the intermolecular stretch frequency increases by ≈14 and 11% upon excitation of ν_s and ν_a of H-bound An$^+$–Ar, respectively. The larger increase upon ν_s excitation is compatible with the larger contribution of the bound N–H stretch local mode to the ν_s normal mode. An alternative assignment of the satellite transitions may be to the $\nu_{s/a}$ fundamentals of a less stable isomer. In this case, the derived red shifts upon complexation would be of the order of 3–4 cm^{-1}, implying that the Ar ligand has a small but noticeable influence on the N–H bonds. As the calculations predict no other isomer (other than the H-bound global minimum) in which the Ar atom is attached to the amino group, an assignment of the satellite transitions to sequence transitions of the H-bound dimer is presently favored over the assignment to $\nu_{s/a}$ of a less stable isomer. Following this scenario, the relative abundance of π-bound and H-bound An$^+$–Ar can roughly be estimated as 1:5 from the ratios of the $\nu_{s/a}$ intensities (≈ 1:8 including the sequence bands, Fig. 4b) and the calculated IR intensities (≈ 0.7, Tab. 1). This result is compatible with the observations for Ph$^+$–Ar, where the relative abundance of the π-bound isomer was estimated as <15% even when the ion source conditions were optimized for the production of this isomer [58].

Figure 4d reproduces the IR spectrum of "hot" An$^+$–Ar dimers generated by 1+1 REMPI of An$^+$–Ar$_2$ and subsequent evaporation of one Ar ligand [53]. Comparison with the REMPI-IR spectrum of "cold" An$^+$–Ar (Fig. 4c) reveals that the spectrum of "hot" An$^+$–Ar shows additional broader bands shifted to the red from the sharp absorptions attributed to the $\nu_{s/a}$ fundamentals of "cold" π-bound An$^+$–Ar. In reference [53] the broad transitions are assigned to sequence transitions of π-bound An$^+$–Ar of the type $\nu_{s/a} + \nu_i \leftarrow \nu_i$, where ν_i are low-frequency intermolecular modes. However, this interpretation cannot be correct because the intermolecular frequencies of π-bound An$^+$–Ar should not depend upon $\nu_{s/a}$ excitation, as the intermolecular interaction potential is essentially the same in the ground and $\nu_{s/a}$ vibrational states (*e.g.*, the small complexation shifts of 1–2 cm^{-1} show that the binding energy changes by less than 0.5%). This view is also supported by the ZEKE spectra of π-bound An$^+$–Ar which reveal that the intermolecular frequencies are nearly independent of excitation of a large variety of intramolecular modes [27,28].

Thus, $\nu_{s/a} + \nu_i \leftarrow \nu_i$ transitions of π-bound An^+–Ar should not be displaced from the $\nu_{s/a}$ fundamentals, in contrast to the observations in Figure 4d where the broad bands are clearly shifted to the red of $\nu_{s/a}$ by some 5–10 cm^{-1}. Comparison of the EI-IR and REMPI-IR spectra in Figures 4b and 4d suggests that the broad bands in the spectrum of hot π-bound An^+–Ar may in fact arise from the H-bound isomer that is produced by an isomerization process which is accompanied by the fragmentation of An^+–Ar_2 into H-bound An^+–Ar and Ar. Briefly, 1+1 REMPI of the (1|1) An–Ar_2 complex ($\pi\pi$ isomer with two π-bound ligands) leads to the production of cold and hot (1|1) An^+–Ar_2 cations where the internal energy is determined by the Franck-Condon factors of the ionization process [27,28]. A significant portion of the produced (1|1) An^+–Ar_2 cations have enough excess energy to overcome the isomerization barrier from the π-bound local minimum to the H-bound global minimum and to evaporate one Ar ligand. The latter process leads to the stabilization of the resulting H-bound dimer *via* evaporative cooling. On the other hand, the spectrum in Figure 4c shows that isomerization from π-bound to a stable deactivated H-bound An^+–Ar is not possible in the case of direct production of π-bound An^+–Ar *via* 1+1 REMPI of An–Ar (Fig. 1), although the excess energy ($\approx$5 600 cm^{-1}) is large enough to overcome the lowest isomerization barrier ($V_b \approx 140$ cm^{-1}). In this case, the FC factors allow only for minor intermolecular excitation (<70 cm^{-1} in the bending mode ν_{bx} along the isomerization coordinate [27,28]) which is not sufficient to overcome the isomerization barrier. Moreover, additional excitation of FC active intramolecular modes leads eventually to predissociation which also prevents the production of a stable H-bound An^+–Ar dimer. In contrast, REMPI of the (1|1) An–Ar_2 trimer followed by fragmentation-assisted isomerization appears to be an efficient scheme to produce stable H-bound An^+–Ar cations starting from neutral An–Ar_n complexes ($n > 1$) because fragmentation can remove internal energy of the cation complex after isomerization has occurred. Actually, the broader bands in the REMPI-IR spectrum of hot An^+–Ar attributed to H-bound An^+–Ar (Fig. 4d) are shifted by a few cm^{-1} to the blue with respect to the corresponding $\nu_{s/a}$ fundamentals of cold H-bound An^+–Ar in the EI-IR spectrum (Fig. 4b) and overlap with the $\nu_{s/a} + \nu_i \leftarrow \nu_i$ sequence transitions assigned to hot H-bound An^+–Ar (Tab. 2). Apparently, evaporative cooling does not completely remove all intermolecular excitation.

The remaining band in the EI-IR spectrum of An^+–Ar at 3 270 cm^{-1} (Fig. 4a) must be assigned to an overtone vibration or a combination band. A similar transition was previously observed in the IR spectra of related An^+–L dimers and tentatively attributed to an overtone of either the NH_2 bending or a ring stretching vibration [12,13]. In the present work the 3 270 cm^{-1} transition is assigned to the first overtone of the symmetric in-plane bending mode of the NH_2 group, $2\nu_b(NH_2)$. The experimental ν_b fundamental of bare An^+ can be approximated as 1 635 cm^{-1} by the frequencies of π-bound An^+–Ar [31]

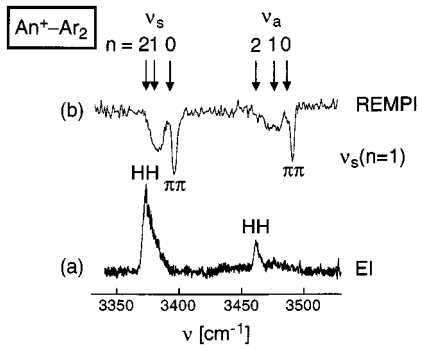

Fig. 5. IR photodissociation spectra of An^+–Ar_2 in the range of the N–H stretch vibrations, ν_s and ν_a. (a) EI-IR spectrum. (b) REMPI-IR spectrum of An^+–Ar_2 generated by 1+1 REMPI of neutral (1|1) An–Ar_2 (reproduced from Ref. [53]). For comparison, the frequencies of the ν_s and ν_a vibrations of An^+, H-bound An^+–Ar, and HH An^+–Ar_2 are indicated by arrows to visualize the incremental red shifts upon sequential Ar complexation at the protons of the amino group. The assignments of the transitions are listed in Table 2.

(the same value is obtained for An^+ embedded in an Ar matrix [54]), and the B3LYP calculations predict high IR intensity and a small blue shift for this mode upon Ar complexation at the H-bound site (+3.5 cm^{-1}). Thus, neglecting anharmonicity $2\nu_b$ is expected near 3 270 and 3 277 cm^{-1} for π-bound and H-bound An^+–Ar, respectively, in good agreement with the experimental value. As the abundance of H-bound An^+–Ar exceeds by far that of π-bound An^+–Ar, the 3 270 cm^{-1} band is mainly attributed to $2\nu_b$ of the former isomer.

4.2 An^+–Ar_2 trimer

Figure 5 compares the IR spectra of An^+–Ar_2 produced in the EI source (a) and by 1+1 REMPI of An–Ar_2 (b [53]). The EI-IR spectrum is dominated by two transitions with band maxima at 3 373 and 3 462 cm^{-1}. Both bands are shifted to lower frequency (by 8 and 13 cm^{-1}, respectively) compared to the corresponding transitions of H-bound An^+–Ar. Consequently, they are assigned to the ν_s and ν_a fundamentals of a planar An^+–Ar_2 trimer featuring two equivalent proton bonds (Fig. 6a, HH isomer, C_{2v} symmetry). This structure corresponds to the global minimum of An^+–Ar_2. The given assignments are confirmed by the observed rotational band contours: both bands are shaded to the blue owing to the contraction of the intermolecular bonds upon vibrational excitation. The degree of shading is similar for both transitions because the two N–H bonds are equivalent in the HH trimer. Moreover, the calculated incremental red shifts with respect to H-bound An^+–Ar ($\Delta\nu_s = -7$ cm^{-1} and $\Delta\nu_a = -11$ cm^{-1}) and ratio of the IR intensities ($\approx$2) are consistent with the experimental observations. The total experimental red shifts of ν_s and ν_a (−20 and −24 cm^{-1}) are also in excellent agreement with the predicted values (−21 and −22 cm^{-1}). In addition, the shifts of the averaged N–H stretch

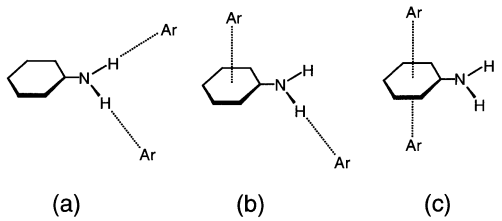

Fig. 6. Isomeric structures of An$^+$–Ar$_2$ in the cation ground state (D_0): (a) planar HH global minimum featuring two equivalent H-bonds (C_{2v} symmetry); (b) Hπ local minimum featuring one H-bond and one π-bond (C_1 symmetry); (c) $\pi\pi$ local minimum featuring two equivalent π-bonds (C_{2v} symmetry).

frequency upon sequential complexation are nearly additive (≈11 cm^{-1} per Ar atom), confirming that the two intermolecular proton bonds are almost equivalent.

Figure 5b reproduces the IR spectrum of An$^+$–Ar$_2$ generated by 1+1 REMPI of neutral (1|1) An–Ar$_2$ ($\pi\pi$ isomer) [53]. The two sharp bands at 3 395.0 and 3 489.8 cm^{-1} are blue-shifted by less than 4 cm^{-1} from the corresponding transitions of bare An$^+$ and thus can safely be assigned to the ν_s and ν_a fundamentals of (1|1) An$^+$–Ar$_2$ (Fig. 6c) [53]. The two broad and relatively intense features in spectrum 5b occurring at 3 382 and 3 475 cm^{-1} "could not sufficiently be explained" in reference [53]. Possible suggestions were sequence transitions of $\nu_{s/a}$ with skeletal vibrations or other isomers [53]. Actually, the positions of these two broad features are close to the ν_s and ν_a fundamentals of H-bound An$^+$–Ar (at 3 381 and 3 477 cm^{-1}). Hence, these bands may arise from the ν_s and ν_a modes of the Hπ An$^+$–Ar$_2$ isomer featuring one H-bond and one π-bond (Fig. 6b). The N–H stretch frequencies of this An$^+$–Ar$_2$ isomer are expected to be similar to those of the H-bound An$^+$–Ar dimer, because the additional π-bond has little influence on the properties of the N–H bonds. Alternatively, the broad bands also overlap with the blue wings of the $\nu_{s/a}$ fundamentals of HH An$^+$–Ar$_2$ and may thus be attributed to hot HH An$^+$–Ar$_2$ isomers. Following these lines, the question arises how the Hπ or HH An$^+$–Ar$_2$ isomers can be formed by ionization of neutral $\pi\pi$ An–Ar$_2$ in reference [53]. In the case of An$^+$–Ar, direct isomerization after ionization without fragmentation is not observed on the time scale of the experiment (the delay between the ionization and IR lasers is 50 ns in Ref. [53]), because the H-bound dimer is not detected in the IR spectrum of An$^+$–Ar produced by 1+1 REMPI of neutral π-bound An–Ar (Fig. 4c). Possibly, the fragmentation process in An$^+$–Ar$_2$ is slower than (or of the order of) 50 ns so that Hπ and HH An$^+$–Ar$_2$ isomers can be observed in the IR spectrum. Another possible way to detect the Hπ or HH trimer isomers in a REMPI-IR spectrum is by ionization of An–Ar$_n$ with $n > 2$. Indeed, REMPI spectra of larger An–Ar$_n$ clusters with $n > 2$ show absorptions at frequencies resonant to the S_1 origin of $\pi\pi$ An–Ar$_2$ [38]. Thus, it is also feasible that the broad bands in the REMPI-IR spectrum of An$^+$–Ar$_2$ arise from the HH or Hπ An$^+$–Ar$_2$ isomers which are created by (near) resonant ionization of neutral An–Ar$_{2+m}$ clusters ($m > 0$) followed by isomerization and evaporation of m ligands.

The EI-IR spectrum of An$^+$–Ar$_2$ is dominated by the ν_s and ν_a fundamentals of the most stable HH An$^+$–Ar$_2$ trimer and does not show any convincing evidence for the presence of less stable isomers. However, it cannot be completely ruled out that a minor part of the signal in the blue wings of the HH isomer absorptions arises from the Hπ and/or $\pi\pi$ isomers. The dominance of the HH An$^+$–Ar$_2$ isomer in the EI-IR spectrum provides further evidence that the proton bonds in An$^+$–Ar$_n$ clusters are more stable than the π-bonds, in agreement with the *ab initio* calculations. This situation is similar to Ph$^+$–Ar$_n$, where the π-bound local minimum was observed for $n = 1$ but the $\pi\pi$ trimer could not be detected in the EI-IR spectrum [60].

4.3 Further discussion

Comparison between An–Ar and An$^+$–Ar demonstrates the dramatic effect of ionization on the intermolecular interaction. The attraction in the neutral An–Ar dimer is dominated by dispersion forces which favor π-bonding over H-bonding. In contrast, the additional charge-induced dipole interaction arising from the extra charge favors the proton-bound structure in the An$^+$–Ar cation. At the present stage, it is not clear whether the H-bound or π-bound structure is more stable in the S_1 state of the dimer. As the amino protons of An are more acidic in the S_1 state than in S_0, the energy difference between the H-bound and π-bound An–Ar minima will probably become smaller (and possibly change sign) upon $S_1 \leftarrow S_0$ excitation. The regular intermolecular vibrational structure observed in the S_1 and D_0 states of π-bound An–Ar suggests that both minima are well separated by significant potential barriers in both electronic states. According to the calculations and the EI-IR spectra, the most stable structure of An$^+$–Ar$_2$ has two equivalent proton bonds and is thus rather different from the most stable (1|1) neutral isomer which has two equivalent π-bonds. The *ab initio* PES of An$^+$–Ar suggests that the microsolvation of An$^+$ in argon will probably proceed by solvating the planar HH An$^+$–Ar$_2$ trimer core by π-bound ligands. The IR spectra reveal that the intermolecular H–Ar proton bonds significantly destabilize the intramolecular N–H bonds, whereas π-bound Ar ligands have only a small and stabilizing effect on the N–H bonds. Unfortunately, the IR spectrum of An$^+$ in an argon matrix has not been recorded in the N–H stretching range [54]. Thus, a comparison of the An$^+$–Ar$_{1,2}$ cluster data with the bulk limit is not possible at the present stage.

The ionization-induced reversal in stability of H-bound and π-bound dimers composed of a rare gas atom and an aromatic molecule featuring a polar acidic subsituent appears to be a very general trend. The Ph$^+$–Ar cation (OH group) was the first such complex for which the H-bound structure was shown to be the global minimum and more stable than the π-bound structure [58–60].

A similar situation is found for isoelectronic An^+–Ar (NH_2 group) in the present work. In contrast, despite numerous spectroscopic and theoretical studies, no example of a H-bound complex between Ar and a neutral aromatic molecule has been identified so far.

The large change in the topology of the intermolecular PES upon ionization is rather common for weakly bound complexes, because the additional charge changes the origin of the dominant attractive interaction. This effect has important consequences for all cluster ion spectroscopic techniques that are based on REMPI of the neutral precursor, because vertical transitions with nonvanishing FC intensity lead in many cases either to the population of repulsive parts (*e.g.*, $C_6H_6^+$–H_2O [70]) or local minima of the cation PES (*e.g.*, An^+–Ar or Ph^+–Ar [60]) but not the global minima. As a consequence, often wrong conclusions may be (and have been) drawn for the properties of the most stable cluster ion structures, such as geometries, adiabatic ionization potentials, dissociation energies, etc. (see discussions in Refs. [60,70]). In contrast, the EI ion source appears to be more generally applicable for the spectroscopy of cold cluster ions because it generates predominantly the most stable isomer of a given cluster ion. For example, in the case of An^+–$Ar_{1,2}$, mainly the most stable proton-bound structures are observed in the EI-IR spectra. These global minima have escaped previous detection in numerous spectroscopic studies using REMPI photoionization techniques (such as PIE [38,55–57], ZEKE [27–29], and REMPI-IR spectroscopy [31,53]).

Previous studies demonstrated that for proton-bound complexes, XH^+–Ar, the intermolecular interaction is correlated to the proton affinity of the base X, PA(X) [10,68,71]. The smaller PA(X), the stronger and shorter the intermolecular bond and the larger the red shift in the X–H stretching frequency. For example, as the PA of C_6H_5O is smaller than that of C_6H_5NH (873 *vs.* 950 kJ/mol [72,73]), the intermolecular proton bond in H-bound Ph^+–Ar [58] is calculated to be stronger than in H-bound An^+–Ar (D_e = 656 *vs.* 513 cm^{-1}). Correspondingly, the shift in the O–H stretch mode in Ph^+–Ar ($\Delta\nu_1 = -70$ cm^{-1} or 2.0% [60]) is larger than those of the N–H stretch modes in An^+–Ar ($\Delta\nu_{s/a} \approx -12$ cm^{-1} or 0.3%). The shifts in An^+–Ar are somewhat smaller than expected from PA(C_6H_5NH) alone, because Ar complexation does not completely remove the relatively strong coupling between the two local N–H stretch oscillators [74]. Similar to related XH^+–Ar cations [75], the attraction in H-bound An^+–Ar is largely dominated by induction forces. According to the AIM population analysis, the H atoms of the amino group carry a large positive partial charge (+0.5*e*). Hence, the H-bound global minima of An^+–Ar can easily be rationalized by the possibility for the polarizable Ar ligand to closely approach the highly concentrated positive charge on the NH_2 protons.

Comparison between NH_3^+–Ar [74,76] and An^+–Ar ($C_6H_5NH_2^+$–Ar) reveals the effect of substitution of a H atom by a phenyl group on the interaction of an amine cation with Ar. Both complexes feature proton-bound equilibrium structures with (nearly) linear H-bonds. However, as the PA of HNH is significantly smaller than that of C_6H_5NH (773 *vs.* 950 kJ/mol [73]), the proton bond in NH_3^+–Ar is significantly stronger and shorter than in An^+–Ar, leading to larger red shifts in the proton donor N–H stretch modes. For example, the intermolecular bonds in H-bound NH_3^+–Ar and An^+–Ar are characterized by R_e = 2.23 and 2.53 Å and D_e = 949 and 513 cm^{-1} at the UMP2/6-311G(2df, 2pd) level, respectively. The major difference between NH_3^+ and An^+ is the shape of the partially filled highest occupied molecular orbital [77]. Ionization of NH_3^+ occurs by ejection of an electron from the $2p_z$ orbital of N. Thus, in addition to the H-bound global minimum, the NH_3^+–Ar potential features a shallow *p*-bound (or N-bound) local minimum in which the Ar ligand is attached to the $2p_z$ orbital of N (C_{3v} symmetry) [74,76]. In contrast, ionization of An to the D_0 state removes a π-electron from the aromatic ring. Hence, the An^+–Ar dimer features a π-bound local minimum, whereas the N-bound structure is close to a transition state (Fig. 3). According to the AIM population analysis, significant positive charge occurs also on the C atom adjacent to the NH_2 group because of the interaction between the nitrogen lone pair and the aromatic π-electron system (partial conjugation). Consequently, the Ar atom in π-bound An^+–Ar is shifted toward the amino group. The microsolvation of both An^+ and NH_3^+ in argon begins with the formation of equivalent intermolecular proton bonds. After all protons are solvated, Ar ligands occupy less favorable binding sites: *e.g.*, π-bonds in An^+–Ar_n ($n > 2$) and *p*-bonds in NH_3^+–Ar_n ($n > 3$) [74,76].

In contrast to previous interpretations [53], the present work strongly suggests alternative assignments of several features in the REMPI-IR spectra of An–$Ar_{1,2}$ which involve fragmentation-assisted isomerization from a π-bound to a H-bound binding site after ionization of neutral An–Ar_2 clusters. This observation appears to be the first spectroscopic identification of such a process in cation clusters of aromatic molecules and nonpolar ligands. A similar ionization-induced isomerization reaction (without subsequent fragmentation) has previously been invoked to explain the REMPI-IR spectra of the aminophenol$^+$–H_2O cation [78]. As the interactions in the neutral and cation clusters are rather different, often significant structural reorganization of solvent molecules occur after ionization of the chromophore molecule. This effect may have important consequences for biomolecular recognition processes.

5 Concluding remarks

The intermolecular interaction in An^+–$Ar_{1,2}$ complexes is investigated for the first time by EI-IR spectroscopy and quantum chemical calculations. These complexes serve as model systems for characterizing the biophysical interaction between charged amines and nonpolar hydrophobic ligands. The analysis of the IR photodissociation spectra in the vicinity of the N–H stretch vibrations unambiguously shows that the Ar ligands prefer H-bonding to the amino group of An^+ over π-bonding to the aromatic ring,

consistent with the results of the *ab initio* calculations. This observation is in stark contrast to all previous spectroscopic studies of An^+–$Ar_{1,2}$ which are based on REMPI of the neutral clusters and only observe the less stable π-bound isomers. Particularly, the REMPI-IR spectra of An^+–$Ar_{1,2}$ are strikingly different from the corresponding EI-IR spectra, clearly demonstrating the severe limitations of photoionization techniques for the production of the most stable isomers of cluster ions. These restrictions are rather general, because the drastic change in the interaction potential upon ionization often causes the most stable structures of the neutral and cation complex to be rather different. Hence, the Franck-Condon factors for transitions connecting both global minima are nearly vanishing. A new alternative interpretation of the An^+–$Ar_{1,2}$ REMPI-IR spectra suggests that ionization of An–Ar_n clusters may be followed by fragmentation-assisted isomerization from a π-bound to a H-bound binding site. Future efforts are directed to the investigation of this process by time-resolved IR spectroscopy.

Note added in proof

After this paper was submitted, Nakanaga and Ito reported new REMPI-IR spectra of An^+–Ar_n ($n = 1$–2) [79].

This study is part of project No. 20-63459.00 of the Swiss National Science Foundation. OD is supported by the Deutsche Forschungsgemeinschaft *via* a Heisenberg Stipendium (DO 729/1-1). He is grateful for the kind hospitality of M. Fujii and his group during his stay at the Institute for Molecular Science (Okazaki, Japan) where part of this paper was written (JSPS fellowship S-01234). We thank A. Fujii for communicating us the vibrational frequencies of the aniline cation prior to publication.

References

1. P. Hobza, R. Zahradnik, *Intermolecular Complexes: The Role of van der Waals Systems in Physical Chemistry and in the Biodisciplines* (Elsevier, Amsterdam, 1988)
2. G.A. Jeffrey, W. Saenger, *Hydrogen bonding in biological systems* (Springer, Heidelberg, 1991)
3. Special Issue on Protein Folding, Acc. Chem. Res. **31** (1998)
4. L. Stryer, *Biochemistry* (Freeman, New York, 1996)
5. Y. Marcus, *Ion solvation* (Wiley, New York, 1985)
6. J. Israelachvili, *Intermolecular and Surface Forces* (Academic Press, London, 1992)
7. A.W. Castleman, R.G. Keesee, Chem. Rev. **86**, 589 (1986)
8. A.W. Castleman, in *Clusters of Atoms and Molecules II*, edited by H. Haberland (Springer, Berlin, 1994), Vol. 56, p. 77
9. K. Müller-Dethlefs, O. Dopfer, T.G. Wright, Chem. Rev. **94**, 1845 (1994)
10. E.J. Bieske, O. Dopfer, Chem. Rev. **100**, 3963 (2000)
11. M.A. Duncan, Annu. Rev. Phys. Chem. **48**, 69 (1997)
12. K. Ohashi, Y. Inokuchi, H. Itzutsu, K. Hino, N. Yamamoto, N. Nishi, H. Sekiya, Chem. Phys. Lett. **323**, 43 (2000)
13. R.P. Schmid, P.K. Chowdhury, J. Miyawaki, F. Ito, K. Sugawara, T. Nakanaga, H. Takeo, H. Jones, Chem. Phys. **218**, 291 (1997)
14. T. Nakanaga, K. Kawamata, F. Ito, Chem. Phys. Lett. **279**, 309 (1997)
15. M. Schäfer, D.W. Pratt, J. Chem. Phys. **115**, 11147 (2001)
16. M. Quack, M. Stockburger, J. Mol. Spectr. **43**, 87 (1972)
17. D.G. Lister, J.K. Tyler, J.H. Hog, N.W. Larsen, J. Mol. Struct. **23**, 253 (1974)
18. N.W. Larsen, E.L. Hansen, F.M. Nicolaisen, Chem. Phys. Lett. **43**, 584 (1976)
19. R.A. Kydd, P.J. Krueger, Chem. Phys. Lett. **49**, 539 (1977)
20. J.M. Hollas, M.R. Howson, T. Ridley, L. Halonen, Chem. Phys. Lett. **98**, 611 (1983)
21. W.E. Sinclair, D.W. Pratt, J. Chem. Phys. **105**, 7942 (1996)
22. I. Lopez-Tocon, R.G. Della Valle, M. Becucci, E. Castellucci, J.C. Otero, Chem. Phys. Lett. **327**, 45 (2000)
23. N. Mikami, A. Hiraya, I. Fujiwara, M. Ito, Chem. Phys. Lett. **74**, 531 (1980)
24. E.R.T. Kerstel, M. Becucci, G. Pietraperzia, E. Castellucci, Chem. Phys. **199**, 263 (1995)
25. M.A. Smith, J.W. Hager, S.C. Wallace, J. Chem. Phys. **80**, 3097 (1984)
26. J.T. Meek, E. Sekreta, W. Wilson, K.S. Viswanathan, J.P. Reilly, J. Chem. Phys. **82**, 1741 (1985)
27. X. Zhang, J.M. Smith, J.L. Knee, J. Chem. Phys. **97**, 2843 (1992)
28. M. Takahashi, H. Ozeki, K. Kimura, J. Chem. Phys. **96**, 6399 (1992)
29. J.G. Jäckel, H. Jones, Chem. Phys. **247**, 321 (1999)
30. X. Song, M. Yang, E.R. Davidson, J.P. Reilly, J. Chem. Phys. **99**, 3224 (1993)
31. H. Piest, G. von Helden, G. Meijer, J. Chem. Phys. **110**, 2010 (1999)
32. J.L. Lin, W.B. Tzeng, J. Chem. Phys. **115**, 743 (2001)
33. K. Yamanouchi, S. Isogai, S. Tsuchiya, K. Kuchitsu, Chem. Phys. **116**, 123 (1987)
34. D. Consalvo, V. Storm, H. Dreizler, Chem. Phys. **228**, 301 (1998)
35. V. Storm, H. Dreizler, D. Consalvo, Chem. Phys. **237**, 395 (1998)
36. M. Becucci, G. Pietraperzia, N.M. Lakin, E. Castellucci, P. Bréchignac, Chem. Phys. Lett. **260**, 87 (1996)
37. E.J. Bieske, A.S. Uichanco, M.W. Rainbird, A.E.W. Knight, J. Chem. Phys. **94**, 7029 (1991)
38. P. Hermine, P. Parneix, B. Coutant, F.G. Amar, P. Bréchignac, Z. Phys. D **22**, 529 (1992)
39. P. Parneix, N. Halberstadt, P. Bréchignac, F.G. Amar, A. van der Avoird, J.W.I. van Bladel, J. Chem. Phys. **98**, 2709 (1993)
40. P. Parneix, P. Bréchignac, J. Chem. Phys. **108**, 1932 (1998)
41. I. Lopez-Tocon, J.C. Otero, M. Becucci, G. Pietraperzia, E. Castellucci, Chem. Phys. **249**, 113 (1999)
42. I. Lopez-Tocon, J.C. Otero, M. Becucci, G. Pietraperzia, E. Castellucci, P. Bréchignac, Chem. Phys. **269**, 29 (2001)
43. A. Amirav, U. Even, J. Jortner, B. Dick, Mol. Phys. **49**, 899 (1983)
44. E.J. Bieske, M.W. Rainbird, I.M. Atkinson, A.E.W. Knight, J. Chem. Phys. **91**, 752 (1989)

45. M.R. Nimlos, M.A. Young, E.R. Bernstein, D.F. Kelley, J. Chem. Phys. **91**, 5268 (1989)
46. P.M. Maxton, M.W. Schaeffer, S.M. Ohline, W. Kim, V.A. Venturo, P.M. Felker, J. Chem. Phys. **101**, 8391 (1994)
47. S. Douin, P. Bréchignac, J. Chim. Phys. **92**, 283 (1995)
48. S. Douin, P. Parneix, F.G. Amar, P. Bréchignac, J. Phys. Chem. A **101**, 122 (1997)
49. S.R. Haines, C.E.H. Dessent, K. Müller-Dethlefs, J. Electr. Spectrosc. Relat. Phenom. **108**, 1 (2000)
50. E.J. Bieske, M.W. Rainbird, A.E.W. Knight, J. Chem. Phys. **94**, 7019 (1991)
51. M. Schmidt, M. Mons, J. Le Calve, Z. Phys. D **17**, 153 (1990)
52. P. Parneix, P. Bréchignac, F.G. Amar, J. Chem. Phys. **104**, 983 (1996)
53. T. Nakanaga, F. Ito, J. Miyawaki, K. Sugawara, H. Takeo, Chem. Phys. Lett. **261**, 414 (1996)
54. C. Gee, S. Douin, C. Crepin, P. Bréchignac, Chem. Phys. Lett. **338**, 130 (2001)
55. S. Douin, P. Parneix, P. Bréchignac, Z. Phys. D **21**, 343 (1991)
56. S. Douin, P. Hermine, P. Parneix, P. Bréchignac, J. Chem. Phys. **97**, 2160 (1992)
57. S. Douin, S. Piccirillo, P. Bréchignac, Chem. Phys. Lett. **273**, 389 (1997)
58. N. Solcà, O. Dopfer, Chem. Phys. Lett. **325**, 354 (2000)
59. N. Solcà, O. Dopfer, J. Mol. Struct. **563/564**, 241 (2000)
60. N. Solcà, O. Dopfer, J. Phys. Chem. A **105**, 5637 (2001)
61. A. Fujii, T. Sawamura, S. Tanabe, T. Ebata, N. Mikami, Chem. Phys. Lett. **225**, 104 (1994)
62. A. Fujii, M. Miyazaki, T. Ebata, N. Mikami, J. Chem. Phys. **110**, 11125 (1999)
63. S.A. Nizkorodov, O. Dopfer, T. Ruchti, M. Meuwly, J.P. Maier, E.J. Bieske, J. Phys. Chem. **99**, 17118 (1995)
64. G. Guelachvili, K.N. Rao, *Handbook of Infrared Standards* (Academic Press, London, 1993)
65. M.J. Frisch *et al.*, *Gaussian 98, Revision A.5.*, Gaussian, Inc, Pittsburgh PA (1998)
66. S.F. Boys, F. Bernardi, Mol. Phys. **19**, 553 (1970)
67. A. Fujii, private communication, December 2001
68. O. Dopfer, D. Roth, J.P. Maier, J. Phys. Chem. A **104**, 11702 (2000)
69. R.V. Olkhov, S.A. Nizkorodov, O. Dopfer, Chem. Phys. **239**, 393 (1998)
70. N. Solcà, O. Dopfer, Chem. Phys. Lett. **347**, 59 (2001)
71. R.V. Olkhov, O. Dopfer, Chem. Phys. Lett. **314**, 215 (1999)
72. H. Kim, R.J. Green, J. Qian, S.L. Anderson, J. Chem. Phys. **112**, 5717 (2000)
73. E.P.L. Hunter, S.G. Lias, J. Phys. Chem. Ref. Data **27**, 413 (1998)
74. O. Dopfer, N. Solcà, R.V. Olkhov, J.P. Maier, Chem. Phys. (in press, 2002)
75. O. Dopfer, J. Phys. Chem. A **104**, 11693 (2000)
76. O. Dopfer, Chem. Phys. (in press, 2002)
77. T.P. Debies, J.W. Rabalais, J. Elec. Spec. Relat. Phenom. **1**, 355 (1972/73)
78. M. Gerhards, C. Unterberg, Appl. Phys. A **72**, 273 (2001)
79. T. Nakanaga, F. Ito, Chem. Phys. Lett. **355**, 109 (2002)